On the Application of Modal Transient Analysis for Online Fault Localization in HVDC Cable Bundles

Ashouri, Mani; Silva, Filipe Miguel Faria da; Bak, Claus Leth

Published in:
I E E E Transactions on Power Delivery

DOI (link to publication from Publisher):
10.1109/TPWRD.2019.2942016

Publication date:
2020

Document Version
Accepted author manuscript, peer reviewed version

On the Application of Modal Transient Analysis for Online Fault Localization in HVDC Cable Bundles

Mani Ashouri, *Student Member, IEEE*, F. Faria da Silva, Senior Member, *IEEE* and Claus Leth Bak, Senior Member, *IEEE*

***Abstract*— This paper presents the modal analysis of different HVDC cable bundles. Using modal theory, specific transformation matrices are presented, and the modal equivalent circuits are illustrated. The behavior of the resulting modes is studied in a wide frequency range, the impact of different cable parameters and burial configurations on the modal characteristics are analyzed. A concept for online fault localization in HVDC cable transmission based on the difference between the modal velocities and consequently the arrival times of the modal traveling wave (TW) initial peaks is presented. In this method, modal voltages and currents are used instead of direct measurements and the proposed concept uses one-sided measurement without needing to detect the second TW reflections. Multiple faults are applied to CIGRE HVDC models in PSCAD/EMTDC and the modal analysis is obtained in MATLAB. The impact of different sampling frequencies, fault resistance, fault location and different grounding schemes on the proposed modal fault location principle is analyzed. The theoretical results show the accuracy of the proposed modal fault localization concept for different HVDC cable bundles.**

***Index Terms*— Eigenvalue Analysis, Fault location, HVDC Cables, Modal Theory, Transients, Traveling Waves.**

I. Introduction

High Voltage Direct Current (HVDC) cable transmission is gaining more attention worldwide, mainly due to widespread underground and submarine transmission for offshore wind generation and connecting largescale AC regions using both line-commutated converter (LCC-HVDC) and voltage source converter (VSC-HVDC) based transmission. However, there are technical obstacles to the protection of cables compared to overhead line (OHL)s. In both HVAC and HVDC transmission, detecting and locating faults is more straightforward for OHLs than cables, because of higher attenuation in the cables due to having contact with materials, which have a higher permittivity than air. Additionally, more complex calculations are needed in cable transmission, because of dealing with more coupled conducting layers than OHLs. Moreover, unlike the OHLs, in which the transmission section is visible, it is more difficult to locate the fault for buried underground and submarine cables [1]. Thereupon, developing novel HVDC cable fault location methods, in both offline and online ways, is an important topic that needs to be investigated in order to improve HVDC transmission technology. Having a robust and reliable fault localization method for HVDC cables can save a massive amount of time and expenses in the repair process [2]. Currently, fault location of HVDC cables consists of standard offline methods, like time domain reflectometry (TDR), in which an offline rectangular impulse traveling wave (TW) signal is sent to one end of the cable, and the reflection time is measured [3]. The bridge measurement is another offline fault localization method, which is based on measuring the resistance variations along the faulty cable using Murray loop. A recent publication in offline fault localization in HVDC cables [4], presented an offline time-frequency reflectometry (TFDR) method, which approximates the fault location in HVDC cables based on combined Euclidean, tangent distance and time-frequency analysis. The method was tested on practical cables in real-time and gave results with an acceptable error. Despite the workability of offline fault location methods for HVDC cables, the main disadvantages are the significant time-consuming process and the need for providing external testing equipment [2]. There are also publications investigating online fault detection and localization for both LCC and VSC-HVDC systems, which are mostly based on TWs [5]–[7], the rate of change of voltage (ROCOV) [8] and artificial intelligence [9]. The TW-based techniques depend on the detection of the reflection of the fault waves for one-sided measuring, which is hard to detect considering the interference of several reflection and refractions particularly for faults close to the measuring location.

Considering that several conducting layers exist in HVDC cables, there can be multiple measurement methods, which may be useful for fault detection and allocation. Most of the researches use directly measured fault data from core conductors [10] and studies also exist using directly measured sheath voltages [11]. However, due to multiple loops in the cable layers, the measured voltages and currents are coupled particularly at low frequencies. They can be transformed into the decoupled modal values that contain accurate information about the attenuation, speed and the arrival time of the fault transient data. Consequently, these modal values can be used for fault detection and localization, which can give more accurate results than directly using coupled pole values. Modal analysis is a well-known method for decoupling n-conductor systems. It is based on eigenvalue theory and it is used to diagonalize matrices with off-diagonal elements. Regarding the cable studies, modal theory deals with the decoupling process

[A]All authors are with the Department of Energy Technology, Aalborg University, Aalborg, Denmark. (e-mail: maa@et.aau.dk, ffs@et.aau.dk, clb@et.aau.dk)

of conducting layers and going from the phase values to the modal values. Each of the modes have specific attenuation, velocity and arrival time to the measurement point [12]. There are studies that use the modal analysis in a way that consider only main conductor and ground modes, which is mostly proper for OHL transmission [13]. Recent works regarding the traveling wave-based fault location of HVDC links, tried to use this method of modal analysis for designing fault locator for OHLs, which use the arrival time delay between conductor and ground modes [14]. The authors concluded that this method is feasible only for long OHLs. However, in cable transmission, the modal velocities are slower than OHLs, and it is possible to detect the initial peaks for closer locations. Additionally, using conductor and ground modes may not be feasible for fault location, because the detection of initial peak for the ground mode is challenging compared to intersheath and interarmour modes, which will be introduced in this paper for HVDC cable transmission.

In HVAC cables, due to cross-bonding, accurate detection of the modes is challenging. Each mode generates other modes at the end of each section due to the change in the forward impedance. Thereupon, there are several modal transient interferences at the end of the cable. Regarding the HVDC cables, there is no cross-bonding and the external cable layers are usually bonded in the two ends. Thus, the modes can be distinguished easier. In this paper, the modal analysis of HVDC cables based on eigenvalue theory is presented. The contributions of this paper are as follows:

1) Studying the modal analysis of HVDC cable bundles. It gives detailed information about the modal characteristics of transients in the time and frequency domain. Most of the modal studies in HVDC cables, simply consider only coaxial and ground modes. This paper gives detailed characteristics for all modes in HVDC cables.
2) Different HVDC cable layer constructions and HVDC cable bundles used in current practical HVDC topologies, including innovative construction with the integrated return are considered and the modal matrices are developed for each construction. Specific transformation matrices are proposed for each bundle in order to convert the directly measured data into the modal value. The equivalent circuit diagram of each mode is also presented.
3) Impacts of different parameters regarding the geometric and materialistic configurations of the cable bundles and the burial and grounding configurations on the modal characteristics are extensively studied.
4) By using the difference in the initial arrival peak of the detected modal transients due to modal velocity difference in HVDC cables, this paper proposes a new TW-based fault location concept for HVDC cable transmission. This technique can be used for online fault localization in HVDC cables requiring only the measured current fault TWs, and the cable data provided by the manufacturer. It does not require external offline pulse injection using commercial cable fault localization technology. The concept uses one-sided current measurement. Additionally, the detection of the second reflection of TWs, which is essential for one-sided fault detection and localization studies, is not necessary. Moreover, different pairs of the modes are possible to be selected and used as a backup, when the detection of the main pair of modes was not successful.

The remainder of this paper is written as follows: section II explains the basics about some of the HVDC cable types, arrangements, and bundles that are used in current installations worldwide. Section III describes the modal theory used for decoupling the longitudinal impedances and voltage and currents. The characteristics of the modes in contrast to frequency and the impact of different parameters are analyzed in section IV and the fault localization concept based on the modal velocity difference is proposed in section V. Section VI discusses some of the considerations for the proposed principle. Finally, the conclusions are given in section VII.

II. HVDC Cable Types

A. HVDC Cable Materials

There are three major HVDC cable types used in current installations, namely: Mass-impregnated (MI), Self-Contained Fluid-Filled (SCFF), and Extruded cables. The main difference is the materials used in cable layers, particularly for insulation layers [15]. The resistivity and permeability of conducting and insulating layers may have a significant impact on the transient characteristics of fault currents and voltages.

B. HVDC cable Arrangements

According to the HVDC topology used, different cable arrangements can be considered. The majority of them are categorized as follows:

1) Two core coaxial cables

In this study, coaxial cables are considered to have a core and a screen layer as conducting layers that are separated by an insulation layer. The two core coaxial (TCC-HVDC) cable bundle consists of two coaxial HVDC cables with the mentioned construction, which is depicted in Fig.1 (a).

2) Single core extruded with metallic return

In HVDC transmission, a metallic return path can be bundled with the main transmission cable instead of using sea or ground as the return. This can be mainly used for asymmetric monopole configuration like Neptune regional transmission system [16] The so-called single core extruded with metallic return (SCEMR-HVDC) cable is depicted in Fig.1(b). In this construction, an armor is considered for the return coaxial cable instead of the screen.

3) Two core extruded cables

This arrangement is very common and it is mainly used for symmetric monopole configurations and symmetric bipole with ground return. The KontiSkan1 link between Denmark and Sweden, the Kontek link between Denmark and Germany and the NordNed HVDC cable between Norway and Netherland [17] are early and late examples for this arrangement. Fig.1 (c) shows the construction of two core extruded (TCE-HVDC) cable.

4) Extruded with integrated metallic return cables

Other than conventional cable bundles, there also some installations with innovative configurations that bring new transmission possibilities for HVDC cable systems. The installed HVDC cable between Ireland and Scotland in 2002 has an integrated metallic coaxial layer as the return path that has many benefits to conventional cables, like better mechanical properties and armoring, less external magnetic field and more compact laying properties [17]. Fig. 1 (d) depicts the construction of extruded with integrated metallic return (EIMR-HVDC) cable.

This article has been accepted for publication in a future issue of this journal, but has not been fully edited. Content may change prior to final publication. Citation information: DOI 10.1109/TPWRD.2019.2942016, IEEE Transactions on Power Delivery

There are other HVDC cable bundle possibilities that can be designed with more complex modal arrangements. As an example, the symmetric bipole with metallic return can consist of two extruded conductors and a coaxial return in a bundled package. However, they are still not practically produced and installed and thus are skipped in this paper.

III. Modal Analysis of HVDC Cables

A. Loops in Various Cable Constructions

Considering multiple conducting layers of cables that are buried underground/sea and various bonding methods, there are a number of loops based on the cable layer arrangement. This makes cable analysis more complex than for OHLs with fewer conducting layers [18]. The current flowing in each layer circulates in a loop with the neighbor outer layer. The procedure of building impedance and admittance matrices for both HVAC and HVDC cables are the same and are given in textbooks and papers [12], [15], [18] and will be skipped in this paper. Fig. 2(a-c) illustrates the loops for HVDC cables with two (TCE-HVDC), three (TCE-HVDC) and four (EIMR-HVDC) conducting layers, respectively. According to the loop impedances, a relation between loop voltage and currents is expressed as:

$$\boldsymbol{V_L} = \boldsymbol{Z_L}.\boldsymbol{I_L} \tag{1}$$

Where, $\boldsymbol{Z_L}$, $\boldsymbol{V_L}$ and $\boldsymbol{I_L}$ are loop impedance, voltage and current matrices, respectively. According to Fig. 2, $\boldsymbol{V_L}$ and $\boldsymbol{I_L}$ matrices will be determined based on the cable layers, given in the black and red parameters, respectively. Eq. (1) needs to be converted from loop to series parameters for modal analysis. According to the well-known coaxial cylindrical conductors theory, the transformation matrices for converting loop impedance matrix to series impedance matrix are given in Eq. (2) as $\boldsymbol{T_1}$, $\boldsymbol{T_2}$, $\boldsymbol{T_3}$, and $\boldsymbol{T_4}$ for TCC-HVDC, SCEMR-HVDC, TCE-HVDC and EIMR-HVDC cables, respectively. Each row of the transformation matrix corresponds to one cable layer. Eq. (3) gives the equation for changing from the loop impedance matrix to series impedance matrix.

$$\boldsymbol{Z_{ph}} = [\boldsymbol{T}]^{-\mathbf{T}}.\boldsymbol{Z_L}.[\boldsymbol{T}]^{-\mathbf{1}} \tag{3}$$

Now the series impedance matrix and pole voltage and current values for each layer are achieved. However, the resulted series impedance matrix will have off-diagonal elements that need to be diagonalized in order to have decoupled values. This is performed by the eigenvalue analysis of the series impedance matrix.

B. Eigenvalue Analysis and the Modal Theory

Modal theory, i.e., eigenvalue analysis has been extensively used in power system stability [12], fault analysis [13], and power electronics control [19]. In overhead lines and cables with distributed parameters modeling, eigenvalue theory is used to have decoupled modal wave propagation parameters. Each mode has specific attenuation, speed, and characteristic

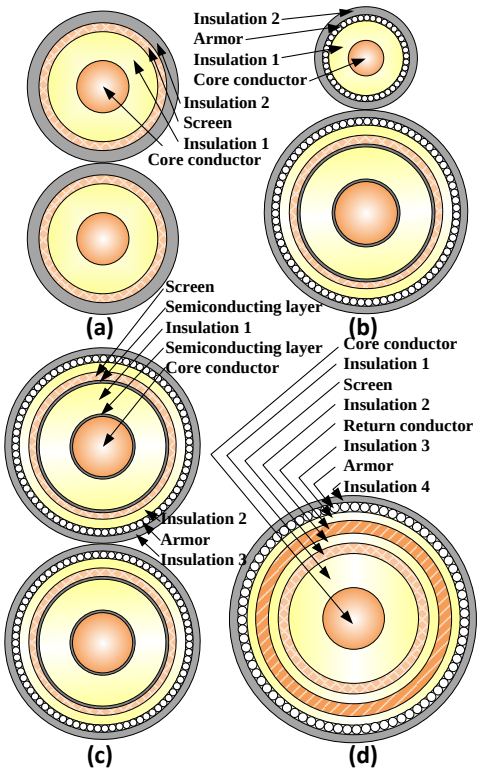

Fig. 1. HVDC cable bundles: (a) Two core coaxial (TCC-HVDC), (b) Single core extruded with metallic return (SCMR-HVDC), (c) Two core extruded (TCE-HVDC), (d) Extruded with integrated metallic return (EIMR-HVDC).

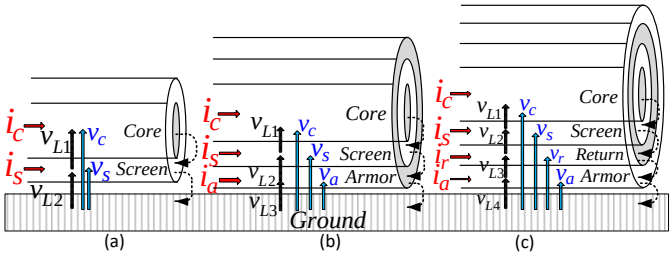

Fig. 2. Loops along cable layers for different HVDC cable constructions. (a): Two conducting layers cable (b): three conducting layers cable (c): Four conducting layers cable.

impedance. The telegraph equations for a transmission line can be written as (4) and (5) [18]:

$$\left[\frac{d^2\boldsymbol{V_p}}{dx^2}\right] = [\boldsymbol{Z_p}][\boldsymbol{Y_p}][\boldsymbol{V_p}] \tag{4}$$

$$\left[\frac{d^2\boldsymbol{I_p}}{dx^2}\right] = [\boldsymbol{Y_p}][\boldsymbol{Z_p}][\boldsymbol{I_p}] \tag{5}$$

Where, $\boldsymbol{Z_p}$ and $\boldsymbol{Y_p}$ are series impedance and admittance matrices based on the pole conductors. The matrix $[\boldsymbol{Z_p}][\boldsymbol{Y_p}]$, which is a non-diagonal matrix, can be written as Eq. (6):

$$[\boldsymbol{Z_p}][\boldsymbol{Y_p}] = \boldsymbol{R\Lambda L} = \boldsymbol{R}\begin{bmatrix}\lambda_1 & 0 & 0 & 0\\ 0 & \lambda_2 & 0 & 0\\ 0 & 0 & \lambda_3 & 0\\ 0 & 0 & 0 & \lambda_4\end{bmatrix}\boldsymbol{L} \tag{6}$$

$$\boldsymbol{T_1} = \begin{bmatrix}1 & 0 & 0 & 0\\ -1 & 1 & 0 & 0\\ 0 & 0 & 1 & 0\\ 0 & 0 & -1 & 1\end{bmatrix} \quad \boldsymbol{T_2} = \begin{bmatrix}1 & 0 & 0 & 0 & 0\\ -1 & 1 & 0 & 0 & 0\\ 0 & 0 & 1 & 0 & 0\\ 0 & 0 & -1 & 1 & 0\\ 0 & 0 & 0 & -1 & 1\end{bmatrix} \quad \boldsymbol{T_3} = \begin{bmatrix}1 & 0 & 0 & 0 & 0 & 0\\ -1 & 1 & 0 & 0 & 0 & 0\\ 0 & -1 & 1 & 0 & 0 & 0\\ 0 & 0 & 0 & 1 & 0 & 0\\ 0 & 0 & 0 & -1 & 1 & 0\\ 0 & 0 & 0 & 0 & -1 & 1\end{bmatrix} \quad \boldsymbol{T_4} = \begin{bmatrix}1 & 0 & 0 & 0\\ -1 & 1 & 0 & 0\\ 0 & -1 & 1 & 0\\ 0 & 0 & -1 & 1\end{bmatrix} \tag{2}$$

This article has been accepted for publication in a future issue of this journal, but has not been fully edited. Content may change prior to final publication. Citation information: DOI 10.1109/TPWRD.2019.2942016, IEEE Transactions on Power Delivery

Where, matrix $\boldsymbol{\Lambda}$, which is a diagonal matrix, is called the eigenvalue or modal matrix and can be found using the characteristic equation of the matrix. Matrix $\boldsymbol{R}$ and $\boldsymbol{L}$ are the right and left eigenvector matrix, respectively and their relation is as (7):

$$\boldsymbol{L} = \boldsymbol{R}^{-1} \tag{7}$$

Accordingly, $\boldsymbol{\Lambda}$ is the modal matrix for$[\boldsymbol{Z_p}][\boldsymbol{Y_p}]$, which can be found using (8):

$$\boldsymbol{\Lambda} = \boldsymbol{R}^{-1}[\boldsymbol{Z_p}][\boldsymbol{Y_p}]\boldsymbol{R} \tag{8}$$

Matrix $\boldsymbol{R}$ will be the eigenvector matrix for voltage transform and it is defined as $\boldsymbol{K_v}$. Then, the modal voltage can be found using (9):

$$[\mathbf{V_m}] = \mathbf{K_v}^{-1}[\mathbf{V_p}] \tag{9}$$

Where, $\boldsymbol{V_m}$ is the modal matrix of voltage. Having the same process, the modal current will be found using (10):

$$[\mathbf{I_M}] = \mathbf{K_i}^{-1}[\mathbf{I_p}] \tag{10}$$

Where, $\boldsymbol{K_i}$ is the current transformation matrix and $\boldsymbol{I_M}$ is the modal matrix of current. The relation between current and voltage transformation matrix will be as:

$$\boldsymbol{K_i} = \boldsymbol{K_v^{-T}} \tag{11}$$

The relation between modal voltage and currents is as (12):

$$[\boldsymbol{V_M}]=[\boldsymbol{Z_M}].[\boldsymbol{I_M}] \tag{12}$$

Then propagation constant can be found as $\sqrt{\boldsymbol{\Lambda}}$, Where, the real part is the attenuation and the imaginary part is called the phase constant. The modal velocity can also be found using (13):

$$\upsilon = \frac{2\pi f}{im(\sqrt{\boldsymbol{\Lambda}})} \tag{13}$$

Where f is frequency and υ is the modal speed.

C. Developing modal matrices for HVDC cable bundles

1) Two core Coaxial cable

In TCC-HVDC cables, a core conductor and a screen layer are considered for each pole. Hence, a total of four modes exist for this bundle. The transformation matrix $\boldsymbol{T_1}$ given in (2) is used to convert the loop impedance matrix to longitudinal series impedance matrix and then the eigenvalue analysis is applied to acquire the modal values. Each of the non-zero elements resulted in the diagonal matrices is an eigenvalue of the series impedance matrix and contains the characteristic information of a specific mode. The modes for this cable are defined as $\boldsymbol{V_M^T} = [\mathrm{V_0}, \mathrm{V_1}, \mathrm{V_2}, \mathrm{V_3}]$ and $\boldsymbol{I_M^T} = [\mathrm{I_0}, \mathrm{I_1}, \mathrm{I_2}, \mathrm{I_3}]$, as voltage and current modes, respectively. The pole voltage and currents are defined as $\boldsymbol{V_P^T} = [\mathrm{V_{c1}}, \mathrm{V_{c2}}, \mathrm{V_{s1}}, \mathrm{V_{s2}}]$ and $\boldsymbol{I_P^T} = [\mathrm{I_{c1}}, \mathrm{I_{c2}}, \mathrm{I_{s1}}, \mathrm{I_{s2}}]$. The first row to the fourth row of the matrix K_{i-TCC} correspond to core 1, core 2, screen 1 and screen 2, respectively. The $\boldsymbol{K_{i-TCC}}$ matrix and the equivalent circuits of the modes are given in Eq. (14) and Fig. 3, respectively (only conducting layers are depicted in all modal figures). The first mode $(\mathrm{V_0}, \mathrm{I_0})$ is a zero-sequence ground mode where the same current in injected into both screens and corresponds to screen-ground loops. It is equivalent to the first column of $\boldsymbol{K_{i-TCC}}$ matrix and is depicted in Fig 3 (a). The second mode $(\mathrm{V_1}, \mathrm{I_1})$ is an intersheath mode where current is flowing in screen-screen loops. This mode corresponds to the second column of $\boldsymbol{K_i}$ and is shown in Fig 3 (b). In the third mode $(\mathrm{V_2}, \mathrm{I_2})$, current is injected into one pole and returns in another pole. This mode is an interconductor mode at lower frequencies and a pure coaxial mode in high frequencies. The third column of $\boldsymbol{K_{i-TCC}}$ and Fig. 3 (c) corresponds to this mode. The fourth mode $(\mathrm{V_3}, \mathrm{I_3})$, is a zero-sequence coaxial mode where current is injected into the core conductors and returns both screens. It corresponds to the fourth column of $\boldsymbol{K_{i-TCC}}$ and is depicted in Fig. 3(d).

$$\boldsymbol{K_{i-TCC}} = \begin{bmatrix} 0 & 0 & \sqrt{2}/2 & \sqrt{2}/2 \\ 0 & 0 & -\sqrt{2}/2 & \sqrt{2}/2 \\ 1 & 1 & -\sqrt{2}/2 & -\sqrt{2}/2 \\ 1 & -1 & \sqrt{2}/2 & -\sqrt{2}/2 \end{bmatrix} \tag{14}$$

2) Single core Extruded with Metallic return

In SCEMR-HVDC cable, there are a total of five modes and the modal voltage and current matrices are $\boldsymbol{V}^T = [\mathrm{V_0}, \mathrm{V_1}, \mathrm{V_2}, \mathrm{V_3}, \mathrm{V_4}]$ and $\boldsymbol{I}^T = [\mathrm{I_0}, \mathrm{I_1}, \mathrm{I_2}, \mathrm{I_3}, \mathrm{I_4}]$, with elements as for coaxial 1, sheath, ground, interarmor and coaxial 2 modes, respectively. The pole voltage and current matrices for this cable model are defined as $\boldsymbol{V_P^T} = [\mathrm{V_{c1}}, \mathrm{V_{c2}}, \mathrm{V_{s1}}, \mathrm{V_{s2}}, \mathrm{V_{a1}}]$ and $\boldsymbol{I_P^T} = [\mathrm{I_{c1}}, \mathrm{I_{c2}}, \mathrm{I_{s1}}, \mathrm{I_{s2}}, \mathrm{I_{a1}}]$ respectively. Therefore, the sequence of the rows of the matrix $K_{i-SCEMR}$ will be as core 1, core 2, screen 1, screen 2 and armor 1. The current modal matrix is given in (15) and the corresponding equivalent circuits are depicted in Fig. 4. The first mode $(\mathrm{V_0}, \mathrm{I_0})$ is a coaxial mode where current is injected into a core and returned in the screen of the same cable. This mode corresponds to the first column of $\boldsymbol{K_{i-SCEMR}}$ and Fig. 4 (a). The second mode $(\mathrm{V_1}, \mathrm{I_1})$ is a sheath mode where current is injected into the screen of the main cable and returns in the armor of the same cable. The second column of $K_{i-SCEMR}$ and Fig. 4 (b) depict this mode. The third mode $(\mathrm{V_2}, \mathrm{I_2})$ is a zero sequence ground mode where the same current is injected into both armors and is returned from the ground. The third column of $\boldsymbol{K_{i-SCEMR}}$ and Fig 4 (c) shows this mode. The fourth mode $(\mathrm{V_3}, \mathrm{I_3})$ is and interarmor mode where current is injected into the armor of the main cable and returns in the armor of the ground return cable. It corresponds to the fourth column of $\boldsymbol{K_{i-SCEMR}}$ and Fig. 4 (d). The last mode $(\mathrm{V_4}, \mathrm{I_4})$ for this cable is a coaxial core mode which is similar to the first mode but for the ground cable.

$$\boldsymbol{K_{i-SCEMR}} = \begin{bmatrix} 1 & 0 & 0 & 0 & 0 \\ 0 & 0 & 0 & 0 & 1 \\ -1 & \sqrt{2} & 0 & 0 & 0 \\ 0 & -\sqrt{2} & 1 & 1 & 0 \\ 0 & 0 & 1 & -1 & -1 \end{bmatrix} \tag{15}$$

3) Two core Extruded cables

In TCE-HVDC cable bundles, three conducting layers exist for each core. Hence, there are a total of six modes with the matrices $\boldsymbol{V}^T = [\mathrm{V_0}, \mathrm{V_1}, \mathrm{V_2}, \mathrm{V_3}, \mathrm{V_4}, \mathrm{V_5}]$ and $\boldsymbol{I}^T = [\mathrm{I_0}, \mathrm{I_1}, \mathrm{I_2}, \mathrm{I_3}, \mathrm{I_4}, \mathrm{I_5}]$, and the polar voltage and current matrices $\boldsymbol{V_P^T} = [\mathrm{V_{c1}}, \mathrm{V_{c2}}, \mathrm{V_{s1}}, \mathrm{V_{s2}}, \mathrm{V_{a1}}, \mathrm{V_{a2}}]$ and $\boldsymbol{I_P^T} = [\mathrm{I_{c1}}, \mathrm{I_{c2}}, \mathrm{I_{s1}}, \mathrm{I_{s2}}, \mathrm{I_{a1}}, \mathrm{I_{a2}}]$, respectively. The columns of $\boldsymbol{K_{i-TCE}}$ correspond to ground $(\mathrm{V_0}, \mathrm{I_0})$, interarmor $(\mathrm{V_1}, \mathrm{I_1})$, coaxial 1 $(\mathrm{V_2}, \mathrm{I_2})$, sheath 1 $(\mathrm{V_3}, \mathrm{I_3})$, coaxial 2 $(\mathrm{V_4}, \mathrm{I_4})$ and sheath 2 $(\mathrm{V_5}, \mathrm{I_5})$ modes, respectively. Coaxial modes are similarly injected into the core and returned to the screen of each pole and the sheath

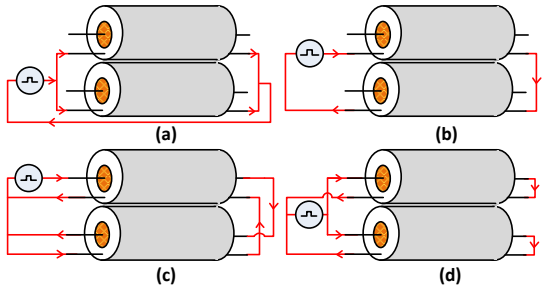

Fig. 3. Equivalent circuits for the modes in TCC-HVDC cables (a): ground (b): intersheath (c): coaxial 1 (d): coaxial 2.

This article has been accepted for publication in a future issue of this journal, but has not been fully edited. Content may change prior to final publication. Citation information: DOI 10.1109/TPWRD.2019.2942016, IEEE Transactions on Power Delivery

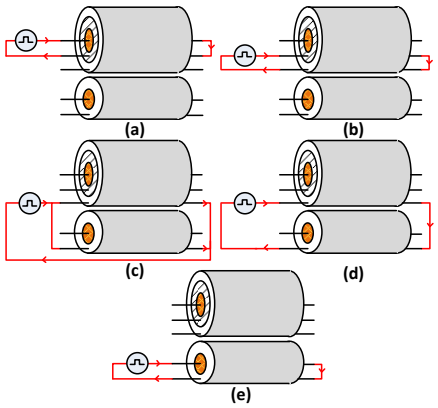

Fig. 4. Equivalent circuits for the modes in SCEMR-HVDC cables (a): coaxial 1 (b): sheath (c): ground (d): interarmor (e): coaxial 2.

modes correspond to screen-armor loops of each pole. The modes are depicted in Fig. 5 and the matrix is given in Eq. (16).

$$\boldsymbol{K_{i-TCE}} = \begin{bmatrix} 0 & 0 & 1 & 0 & 0 & 0 \\ 0 & 0 & 0 & 0 & 1 & 0 \\ 0 & 0 & -1 & \sqrt{2} & 0 & 0 \\ 0 & 0 & 0 & 0 & -1 & \sqrt{2} \\ 1 & 1 & 0 & -\sqrt{2} & 0 & 0 \\ 1 & -1 & 0 & 0 & 0 & -\sqrt{2} \end{bmatrix} \quad (16)$$

4) Integrated metallic return cables

In EIMR-HVDC cable, instead of a separate coaxial metallic return cable, an additional layer exist between sheath and armor as the return path. This layer adds another loop in correspondence to Fig. 2 (c). Hence, there will be a total of four modes with the modal voltages and currents of matrices $\boldsymbol{V}^T = [\mathrm{V_0}, \mathrm{V_1}, \mathrm{V_2}, \mathrm{V_3}, \mathrm{V_4}]$ and $\boldsymbol{i}^T = [\mathrm{I_0}, \mathrm{I_1}, \mathrm{I_2}, \mathrm{I_3}, \mathrm{I_4}]$, with polar matrices as $\boldsymbol{V_P^T} = [\mathrm{V_{c1}}, \mathrm{V_{s1}}, \mathrm{V_{r1}}, \mathrm{V_{a1}}]$ and $\boldsymbol{I_P^T} = [\mathrm{I_{c1}}, \mathrm{I_{s1}}, \mathrm{I_{r1}}, \mathrm{I_{a1}}]$, corresponding to each row of matrix K_{i-EIMR}, respectively.

The first to the fourth columns of K_{i-EIMR} in (17) show coaxial $(\mathrm{V_0}, \mathrm{I_0})$, sheath $(\mathrm{V_1}, \mathrm{I_1})$, ground $(\mathrm{V_2}, \mathrm{I_2})$, and a return mode $(\mathrm{V_3}, \mathrm{I_3})$, respectively. In the return mode, current is injected into the return conductor and is returned in the armor, which is the fourth layer in EIMR-HVDC cable. Fig. 6 depicts the modes for this cable.

$$\boldsymbol{K_{i-EIMR}} = \begin{bmatrix} 1 & 0 & 0 & 0 \\ -1 & \sqrt{2} & 0 & 0 \\ 0 & -\sqrt{2} & 0 & \sqrt{3} \\ 0 & 0 & 2 & -\sqrt{3} \end{bmatrix} \quad (17)$$

D. Modal velocity difference for fault location

Each of the modes for every cable bundle, has a specific attenuation and velocity in different frequencies. The difference in the velocity of the decoupled modes can be used for fault localization in HVDC cable bundles. In HVAC systems, the cables are cross-bonded and the modes have interference at the end of each section. In fact, each mode divides itself into the other modes at the crossing point. The cross-bonding also causes higher modal attenuation, which makes the detection of modes more challenging. However, cross-bonding does not exist in HVDC cables and there is no interference between the modes at any distance in the middle of the cable, except in case of joining points in multi-terminal HVDC links. Thereupon, the detection of modes is feasible in HVDC cable transmission. Considering the difference in the velocity of each mode, they have different arrival times to the measurement location. Due

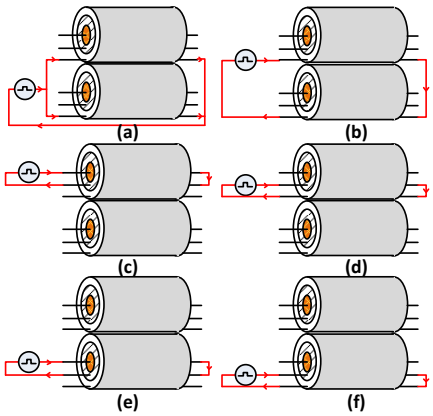

Fig. 5. Equivalent circuits for the modes in TCE-HVDC cables (a): ground (b): interarmor (c): coaxial 1 (d): sheath 1 (e): coaxial 2 (f): sheath 2.

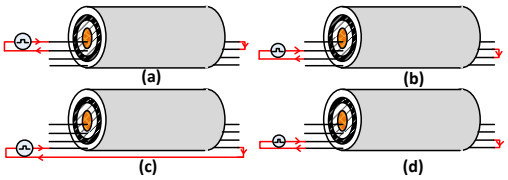

Fig. 6. Equivalent circuits for the modes in EIMR-HVDC cables (a): coaxial (b): sheath (c): ground (d): return.

to the decoupled system of the modes in high frequencies, the fault location using time difference between the modes gives more accurate results than using the arrival time of pole layers. Having the arrival time of the modes, the fault location is determined using the following equation based on one-sided measurement:

$$\mathrm{d} = \frac{\Delta \mathrm{t_{ij}}}{\left(\frac{1}{\upsilon_{\mathrm{j,f}}} - \frac{1}{\upsilon_{\mathrm{i,f}}}\right)} \quad (18)$$

Where, d is the determined fault distance from the measurement location, $\Delta \mathrm{t_{ij}}$ is the arrival time difference between the modes i and j. $\upsilon_{\mathrm{i,f}}$ and $\upsilon_{\mathrm{j,f}}$ are the velocities for modes i and j at the frequency f respectively. Fig. 7 depicts the flowchart for determining $\boldsymbol{K_i}$, modal currents, and fault location.

IV. CHARACTERISTICS OF THE MODES

The pole impedance and admittance matrices and consequently the resulted eigenvalues are complex numbers, which are frequency dependent. In lower frequencies, the modes are coupled and the modal matrices still have small size off-diagonal elements. As the frequency increases, the imaginary part of the eigenvalues gets closer to zero [18]. Table I shows the frequency dependency of the modal attenuation and velocity for all cable bundles. The modal attenuations are the real part of $\sqrt{\boldsymbol{\Lambda}}$ and the modal velocities are calculated using (17). The cable data for different bundles are adopted from [12], [20], [21]. According to the table I, for frequencies higher than 100 kHz, the modal velocities do not change significantly. In high frequencies, the modes are considered as completely decoupled and the frequency of 1 MHz is considered for all modal studies in this paper. The remainder of this section studies the impact of cable dimensional parameters, material properties and burial configurations on the modal characteristics. Due to page limitations, only a number of parameters are studied for each

This article has been accepted for publication in a future issue of this journal, but has not been fully edited. Content may change prior to final publication. Citation information: DOI 10.1109/TPWRD.2019.2942016, IEEE Transactions on Power Delivery

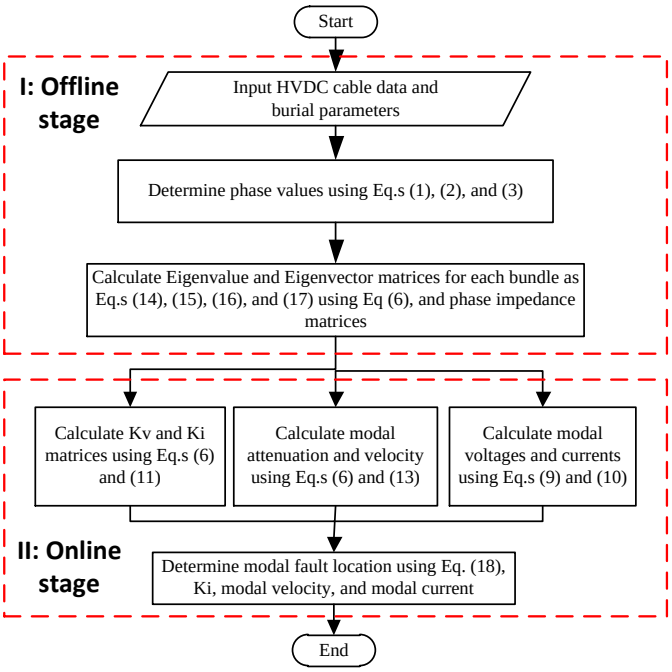

Fig. 7. Flowchart for calculating different parameters explained in section III.

cable bundle. Tables II-V give modal characteristics based on different parameters. The results given in tables II-V are obtained in the frequency of 1 MHz. The highlighted values give the parameters used as the cable bundle data for fault localization in section V.

A. *Impact of dimensional parameters*

Table II shows the impact of dimensional parameters on the modal characteristics of TCC-HVDC cable bundle. According to the results, when the burial depth increases, ground mode attenuation and velocity increase. This leads to a decrease in the attenuation of the intersheath mode, while the intersheath velocity faces a slight increase. The coaxial mode parameters remain constant with different burial depths. When the radius of the core insulation gets larger, the attenuation of the ground and intersheath modes increase, while the coaxial attenuation gets smaller. The ground velocity decreases, while the intersheath and coaxial velocities get larger with an increase in the radius of the core insulation. According to the table, an increase in the sheath radius leads to an increase in the ground mode attenuation and a slight decrease in intersheath attenuation, while the coaxial attenuations remain constant. Increasing the sheath radius, will diminish the velocity of the ground mode and increase the intersheath mode velocity, while the coaxial speeds remain constant. According to the results for the impact of dimensional parameters, they do not have a significant impact on the modal attenuation and velocities and all the mentioned changes are very small, particularly on the coaxial modes.

The impact of different burial angles and the distance between the poles for TCE-HVDC cable are given in table III. As the distance between the two poles increase, both attenuation, and velocity of the ground mode increases, while the attenuation and velocity of the interarmor mode get smaller. The attenuation and velocities for the coaxial and sheath modes remain constant with a small change in the distance between the poles. According to the table, there is not a significant difference in the modal characteristics between different burial angles, namely horizontal, vertical, and with 45◦ angle.

TABLE I: FREQUENCY DEPENDENCY OF MODAL ATTENUATION AND PROPAGATION VELOCITY IN VARIOUS HVDC CABLE BUNDLES

Frequency [Hz]			1K	2K	5K	100K	1M
TCC-HVDC	Att. [dB/Km]	V_0	0.26	0.49	1.21	28.97	**357.35**
		V_1	0.22	0.22	0.22	0.37	**3.75**
		V_2	0.07	0.09	0.11	0.32	**1.04**
		V_3	0.09	0.10	0.11	0.32	**1.04**
	Vel. [$m/\mu s$]	V_0	12.46	12.75	13.15	14.90	**17.11**
		V_1	52.69	49.27	51.43	52.68	**53.60**
		V_2	164.66	181.51	191.22	195.31	**196.93**
		V_3	178.23	181.25	191.22	195.31	**196.93**
SCEMR-HVDC	Att. [dB/Km]	V_0	0.05	0.06	0.07	0.27	**0.86**
		V_1	0.57	0.92	1.72	13.90	**60.15**
		V_2	0.35	0.64	1.46	29.29	**341.94**
		V_3	0.41	0.65	1.16	6.34	**21.59**
		V_4	0.22	0.37	0.67	4.04	**13.89**
	Vel. [$m/\mu s$]	V_0	183.26	188.25	191.31	195.74	**197.06**
		V_1	42.27	50.12	62.15	138.47	**156.35**
		V_2	12.86	13.28	13.86	15.96	**18.45**
		V_3	35.69	39.63	44.40	54.14	**56.72**
		V_4	78.72	89.60	104.18	141.11	**153.30**
TCE-HVDC	Att. [dB/Km]	V_0	0.34	0.62	1.33	26.88	**320.28**
		V_1	0.38	0.59	1.04	5.39	**12.82**
		V_2	0.08	0.09	0.11	0.32	**1.04**
		V_3	0.70	1.10	2.05	16.38	**73.76**
		V_4	0.08	0.09	0.11	0.32	**1.04**
		V_5	0.70	1.10	2.05	16.38	**73.76**
	Vel. [$m/\mu s$]	V_0	14.12	14.59	15.21	17.53	**20.32**
		V_1	38.09	42.09	46.86	56.22	**58.36**
		V_2	175.88	185.21	190.56	195.31	**196.93**
		V_3	36.88	44.02	55.05	104.00	**147.94**
		V_4	175.88	185.21	190.56	195.31	**196.93**
		V_5	36.88	44.02	55.05	144.40	**147.94**
EIMR-HVDC	Att. [dB/Km]	V_0	0.02	0.03	0.04	0.32	**1.03**
		V_1	0.24	0.28	0.78	2.21	**7.47**
		V_2	0.17	0.34	0.94	15.91	**182.78**
		V_3	0.12	0.16	0.32	6.78	**25.43**
	Vel. [$m/\mu s$]	V_0	178.14	181.69	187.87	195.35	**196.94**
		V_1	133.28	152.09	153.67	186.10	**192.33**
		V_2	19.20	19.69	25.35	29.33	**33.82**
		V_3	133.08	139.27	94.87	151.53	**179.61**

B. *Impact of layer material properties*

The impact of different resistivity values for conducting layers of TCE-HVDC cables are given in table IV. An increase in the resistivity of the main conductor will increase the attenuation of coaxial core mode, while slightly decreases its velocity. The rest of the modes will have constant attenuation and velocity with change in the core resistivity. As the sheath resistivity for the main cable increases, modal attenuation for coaxial core and sheath modes get larger and their velocity gets smaller. The attenuation and velocity of the other modes remain constant. An increase in the resistivity of the armor will increase the attenuation of the sheath, ground, and armor modes while decreasing their velocity. According to the results, any change in the resistivity of conductor layers for one of the poles, will not have a significant impact on the coaxial modes of the other pole. In summary, the resistivity of a specific layer will have a direct impact on the attenuation and an opposite impact on the velocity of the modes resulted from the neighbor layers in the same cable.

Table V studies the impact of layer permeability on the modal characteristic of EIMR-HVDC cables. According to the table, an increase in the permeability of the core conductor, will increase the attenuation of the coaxial core and decrease its velocity. No change is observed in the characteristics of the other modes on this test. As the sheath permeability increases, the attenuation of the coaxial and sheath modes increase, while their velocity gets smaller. Any change in the armor permeability also has a direct impact on the attenuation of ground and return modes and opposite impact on their velocity. After extensive tests on the impact of different materials on the characteristics of the modes on different cable bundles, it is observed that the conductor permeability have the most significant impact on the attenuation and speed of the modes among all tested parameters. The most significant impact was for the armor permeability of TCE-HVDC cable. Using different material for the armor and consequently with a change in the armor relative permeability for TCE-HVDC cable from 1 to 400, the modal attenuation significantly increases, which may make the detection of the initial peaks of the modes challenging. Hence, the selected material in TCE-HVDC cable has armor relative permeability of 400, to have the most challenging situation for fault localization case in section VI.

V. Modal velocity Difference For Fault Location

According to the different modes explained in section III and the determined modal velocities in Table I, there are various possibilities between every two modes in each bundle than theoretically can be used for the fault location. The proposed fault localization concept only needs the measured fault data from one side of the cable and there is no need for the communication link. Most of the TW-based fault detection and location techniques that use one-side measurements in both HVAC and HVDC systems, measure the time difference between the first wave arrival time and the second reflection time. In this method, only the initial peak of different pairs of the modes are used for fault localization and there is no need to detect the second reflection of the waves, which is challenging to be accurately detected.

To analyze the fault localization using the proposed modal principle, extensive tests with various configurations are investigated and the impact of different parameters are studied. Each of the proposed cable bundles is used to study a specific parameter. Fig. 8 depicts the single line diagram of CIGRE LCC and VSC HVDC links, which are used for fault analysis. The systems are simulated in PSCAD and the defined faults are applied on different cable bundles. Standard PSCAD current measurement blocks are inserted at the end of each conducting layer in one side of the transmission links. The ammeter placement and the corresponding parameters are shown in Fig. 8. Table VI shows the defined fault scenarios used in different study cases. Technical data can be found in [22] for LCC-HVDC link used for testing SCEMR-HVDC cable and the VSC-HVDC system used for TCC-HVDC and TCE-HVDC cable tests are given in [21]. The cable data for different bundles are adopted from [12], [20], [21]. The cables series impedance and admittance matrices are obtained for the frequency of 1 MHz and the data is exported to MATLAB. Eigenvalue analysis, the related parameters, the modal voltages and currents, and the modal fault location are determined according to the flowchart given in Fig. 7. This paper focuses on the behavior of modes for different HVDC cable bundles in frequency and time domain. In this section, only the principle of the fault localization based on the modal velocity difference is proposed and the time difference between the initial peaks of the modes is studied. The signal processing, which must be used for accurate detection of the modal initial peaks and implementation of the proposed technique to design an online fault localization algorithm is not in the scope of this paper and it is considered as future research. In all study cases, the exact sample that each modal wave faces an increasing change is considered as the initial arrival of the fault transient, which may have a small error based on the sample delays resulted in the signal processing technique used. Impact of different parameters on the accuracy of the proposed modal technique to detect the fault location is studied in the following section.

A. Impact of sampling frequency:

Fault I studies the impact of different sampling frequencies on the modal initial peak arrivals in TCC-HVDC cable. The line length is 400 km and the fault is applied to the middle of the line. According to the coaxial and sheath modal velocities in the frequency of 1 MHZ given in table I, the modal time difference using sampling frequencies of 1 MHz, 40 kHz, and 20 kHz, is depicted in Fig. 9 (a-c), respectively. Table VII gives the modal time different results, determined fault location, and the corresponding relative error. Although the frequency of 1 MHz is used as the default sampling frequency for all cases to shows the most accurate arrival peaks for the modes, the results prove that lower sampling frequencies also give acceptable results for the time difference between the modal initial peaks. However, based on the signal processing techniques used for designing the fault location algorithm, the total sample delays may vary, which is dependent on the accuracy and robustness of the signal processing technique used.

B. Impact of fault resistance

Faults II-IV study the impact of fault resistance on the initial peaks of modes in SCEIMR-HVDC cable. The total length of the cable bundle for this case is 100 km, and all the faults are applied to the middle of the line. Fig. 10 (a-c) depict the modal fault waves for faults I-IV, respectively. According to the figure, for higher impedance faults, the detection of the modal initial peaks will be more challenging for the signal processing method used. However, it is still possible to detect the modal peak arrivals and the initial peaks can still be clearly distinguished from the normal situation in modal fault current wave. Different combination of the modes can be used for locating the fault. The time difference between the initial peaks of coaxial 1- sheath, and coaxial 1- coaxial 2 modes are 63 μs, and 72 μs, respectively. According to the modal speeds in the frequency of 1 MHz given in table I, the determined fault locations are 47.68 and 49.70 km, using the two mentioned combination of the modes. These values can be determined for all three faults regardless of the fault impedance. According to the results, increasing the fault impedance does not have a direct impact on the principle of time difference for different modes. However, it may make the detection of the initial peak more challenging, which can be handled by using more accurate and robust signal-processing techniques.

This article has been accepted for publication in a future issue of this journal, but has not been fully edited. Content may change prior to final publication. Citation information: DOI 10.1109/TPWRD.2019.2942016, IEEE Transactions on Power Delivery

TABLE II: IMPACT OF DIMENSIONAL PARAMETERS ON THE MODAL CHARACTERISTICS OF TCC-HVDC CABLE BUNDLES

Parameter			h [m]					r_{ins} [mm]					r_s [mm]				
Value			↑	0.25	1	1.5	3	↑	10	15	20	25	↑	0.5	1	2	4
TCC-HVDC	Att. [dB/Km]	V_0	↑	305.8	348.1	**357.3**	358.2	↑	314.8	336.6	**357.3**	377.7	↑	351.2	353.3	**357.3**	365.3
		V_1	↓	4.5	3.8	**3.75**	3.73	↑	2.16	3.36	**3.75**	4.07		3.74	3.68	**3.75**	3.88
		V_2	→	1.04	1.04	**1.04**	1.04	↓	2.91	1.40	**1.04**	0.82	→	1.04	1.04	**1.04**	1.04
		V_3	↑	1.04	1.04	**1.04**	1.04	↓	2.91	1.40	**1.04**	0.82	→	1.04	1.04	**1.04**	1.04
	Vel. [$m/\mu s$]	V_0	↑	16.59	16.92	**17.11**	17.46	↓	18.93	17.94	**17.11**	16.38	↓	17.34	17.26	**17.11**	16.80
		V_1	↑	53.56	53.59	**53.64**	53.66	↑	53.15	53.26	**53.60**	54.28	↑	53.46	53.50	**53.60**	53.83
		V_2	→	196.9	196.9	**196.9**	196.9	↑	196.1	196.6	**196.9**	197.1	→	196.9	196.9	**196.9**	196.9
		V_3	→	196.9	196.9	**196.9**	196.9	↑	196.1	196.6	**196.9**	197.1	→	196.9	196.9	**196.9**	196.9

TABLE III: IMPACT OF BURYING CONFIGURATIONS ON THE MODAL CHARACTERISTICS OF TCE-HVDC CABLE BUNDLES

Parameter			Horizontal arrangement [mm]				Vertical arrangement [mm]				45 degree [mm]				
Value			↑	130	١٤٣,٥	١٧٠	٢٠٠	↑	130	١٤٣,٥	١٧٠	٢٠٠	↑	130	١٤٣,٥	١٧٠	٢٠٠
TCE-HVDC	Att. [dB/Km]	V_0	↑	318.2	**320.3**	324.0	327.6	↑	317.5	319.6	323.1	326.5	↑	316.9	318.5	320.6	322.2
		V_1	↓	14.15	**12.83**	10.94	9.51	↓	14.06	12.72	10.80	9.34	↓	14.21	13.68	12.44	11.67
		V_2	→	1.04	**1.04**	1.04	1.04	→	1.04	1.04	1.04	1.04	→	1.04	1.04	1.04	1.04
		V_3	→	73.76	**73.76**	73.76	73.76	→	73.76	73.76	73.76	73.76	→	73.76	73.76	73.76	73.76
		V_4	→	1.04	**1.04**	1.04	1.04	→	1.04	1.04	1.04	1.04	→	1.04	1.04	1.04	1.04
		V_5	→	73.76	**73.76**	73.76	73.76	→	73.76	73.76	73.76	73.76	→	73.76	73.76	73.76	73.76
	Vel. [$m/\mu s$]	V_0	↑	20.20	**20.33**	20.54	20.75	↑	20.18	20.29	20.50	20.70	↑	20.12	20.23	20.35	20.44
		V_1	↓	61.52	**58.36**	53.87	50.42	↓	61.53	58.35	53.88	50.42	↓	62.34	60.45	57.52	55.66
		V_2	→	196.9	**196.9**	196.9	196.9	→	196.9	196.9	196.9	196.9	→	196.9	196.9	196.9	196.9
		V_3	→	147.9	**147.9**	147.9	147.9	→	147.9	147.9	147.9	147.9	→	147.9	147.9	147.9	147.9
		V_4	→	196.9	**196.9**	196.9	196.9	→	196.9	196.9	196.9	196.9	→	196.9	196.9	196.9	196.9
		V_5	→	147.9	**147.9**	147.9	147.9	→	147.9	147.9	147.9	147.9	→	147.9	147.9	147.9	147.9

TABLE IV: IMPACT OF CONDUCTOR LAYERS' RESISTIVITY ON THE MODAL CHARACTERISTICS OF SCEIMR-HVDC CABLE BUNDLES

Parameter			ρ_c [Ωm]					ρ_s [Ωm]					ρ_a [Ωm]				
Value			↑	0.5e-8	1.5e-8	**2.2e-8**	2e-7	↑	10e-8	20e-8	**27e-8**	10e-7	↑	50e-8	80e-9	**18e-8**	10e-7
SCEMR-HVDC	Att. [dB/Km]	V_0	↑	0.69	0.80	**0.86**	1.52	↑	0.64	0.78	**0.86**	1.35	→	0.86	0.86	**0.86**	0.86
		V_1	→	60.15	60.15	**60.15**	60.15	↑	58.95	59.71	**60.15**	62.88	↑	36.65	43.97	**60.15**	110.9
		V_2	→	341.9	341.9	**341.9**	341.9	→	341.9	341.9	**341.9**	341.9	↑	340.9	341.2	**341.9**	344.9
		V_3	→	21.59	21.59	**21.59**	51.59	→	21.59	21.59	**21.59**	21.59	↑	17.00	18.35	**21.59**	34.27
		V_4	→	13.89	13.89	**13.89**	13.89	→	13.89	13.89	**13.89**	13.89	→	13.89	13.89	**13.89**	13.89
	Vel. [$m/\mu s$]	V_0	↓	197.2	197.1	**197.1**	196.6	↓	197.2	197.1	**197.1**	196.7	→	197.1	197.1	**197.1**	197.1
		V_1	→	156.3	156.3	**156.3**	156.3	↓	157.1	156.6	**156.3**	154.6	↓	171.8	166.9	**156.4**	127.4
		V_2	→	18.45	18.45	**18.45**	18.45	→	18.45	18.45	**18.45**	18.45	↓	18.46	18.46	**18.45**	18.43
		V_3	→	56.72	56.72	**56.72**	56.72	→	56.72	56.72	**56.72**	56.72	↓	57.01	56.92	**56.72**	55.92
		V_4	→	153.3	153.3	**153.3**	153.3	→	153.3	153.3	**153.3**	**153.3**	→	153.3	153.3	**153.3**	153.3

TABLE V: IMPACT OF LAYERS' PERMEABILITY ON THE MODAL CHARACTERISTICS OF EIMR-HVDC CABLE BUNDLES

Parameter			μ_c					μ_s					μ_a				
Value			↑	**1**	100	200	400	↑	**1**	100	200	400	↑	1	100	200	**400**
EIMR-HVDC	Att. [dB/Km]	V_0	↑	**1.03**	4.12	5.52	7.48	↑	**1.03**	7.04	9.72	13.42	→	1.03	1.03	1.03	**1.03**
		V_1	→	**7.47**	7.47	7.47	7.47	↑	**7.47**	51.04	67.11	87.05	→	7.47	7.47	7.47	**7.47**
		V_2	→	**182.8**	182.8	182.8	182.78	→	**182.8**	182.8	182.8	182.7	↑	178.2	180.4	181.4	**182.8**
		V_3	→	**25.43**	25.43	25.43	25.43	→	**25.43**	25.43	25.43	25.43	↑	1.91	13.57	18.61	**25.43**
	Vel. [$m/\mu s$]	V_0	↓	**196.9**	194.8	193.7	192.32	↓	**196.9**	192.6	190.7	188.1	→	196.9	196.9	196.9	**196.9**
		V_1	→	**192.3**	192.3	192.3	192.3	↓	**192.3**	162.2	152.0	140.2	→	192.3	192.3	192.3	**192.3**
		V_2	→	**33.82**	33.82	33.82	33.82	→	**33.82**	33.82	33.82	33.82	↓	33.94	33.88	33.86	**33.8**
		V_3	→	**179.6**	179.6	179.6	179.6	→	**179.6**	179.6	179.6	179.6	↓	196.3	187.9	184.4	**179.6**

↑ parameter increase in the row, ↓ parameter decrease in the row, → No parameter change in the row.

C. *Impact of fault location*

Faults V-VII investigate faults in different locations of the system. In this study, coaxial and sheath modes are used for fault localization in a TCE-HVDC cable with the total length of 300 km. The armor material with the relative permeability 400 is used for the model, to have the highest modal attenuation and consequently the most challenging case for initial peak detection. Fig. 11 (a-c) depict the modal fault current waves for faults in 1, 150, and 280 km from the right busbar. The detection results are given in table VIII. According to Fig. 11(a), the arrival time must be about 1.6 μs, for fault happening at 1 km from the right busbar. However, due to the sampling frequency,

This article has been accepted for publication in a future issue of this journal, but has not been fully edited. Content may change prior to final publication. Citation information: DOI 10.1109/TPWRD.2019.2942016, IEEE Transactions on Power Delivery

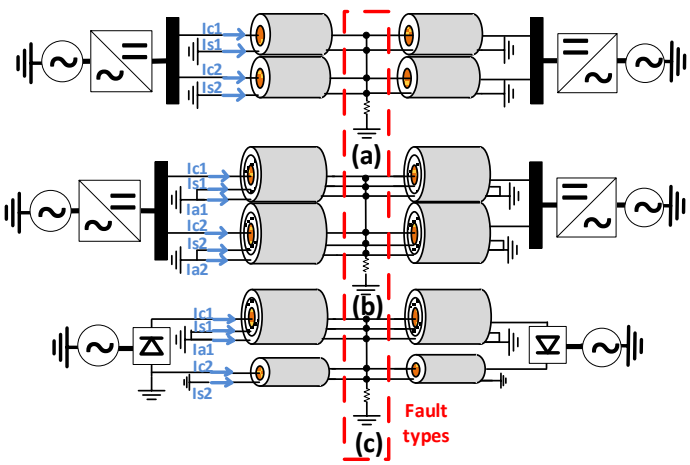

Fig. 8. Single line diagram and the involved layers in the faults for different cable bundles used in simulations (a): TCC-HVDC (b): TCE-HVDC (c): SCEMR-HVDC.

TABLE VI: DEFINED FAULT CASES FOR MODAL FAULT LOCATION STUDY

Fault No.	HVDC type	Cable bundle	Impact of	Fault type	Fault Res. [Ω]	location [km]
I	VSC *	TCC-HVDC	sampling frequency	P2P	0.1	200
II	LCC**	SCEIMR-HVDC	fault resistance	P2R2G	0.1	50
III	LCC	SCEIMR-HVDC	fault resistance	P2R2G	1	50
IV	LCC	SCEIMR-HVDC	fault resistance	P2R2G	100	50
V	VSC	TCE-HVDC	fault location	P2P	100	1
VI	VSC	TCE-HVDC	fault location	P2P	100	150
VII	VSC	TCE-HVDC	fault location	P2P	100	280
IX	VSC	TCE-HVDC	grounding	P2P2G	1	120

*SYMMETRIC MONOPOLE, **WITH METALLIC RETURN

TABLE VII: IMPACT OF SAMPLING FREQUENCY ON THE MODAL ARRIVAL TIME IN TCC-HVDC CABLES

Fault No.	Sampling frequency	Modal time difference [ms]	Determined location [km]	Relative error [%]
I	**1 MHz**	2.715	199.944	-0.028
I	**40 kHz**	2.725	200.680	0.34
I	**20 kHz**	2.750	202.522	1.26

the detected time is 2 μs, which gives the absolute relative error of 18.9%. This high error value is not related to the modal fault location principle and can be reduced using higher sampling frequencies. This high error value does not exist in fault cases VI, and VII, which are applied far from the measurement location. However, the detection of initial arrival peak in the modal fault current wave is challenging particularly for fault VII, which is applied 280 km far from the measuring point and close to the remote busbar. Again, in this case, using a robust and accurate signal-processing technique can detect the initial increase in the modal current wave with minimum additional sample delays.

D. Impact of grounding scheme

In this section fault IX is applied to the TCE-HVDC cable to study the impact of different grounding schemes on the behavior of the modes and consequently the feasibility of the modal fault localization principle. Three types of grounding schemes are considered for TCE-HVDC cable. In the first case, screen and armor are grounded only in two sides of the cable with 0.1 Ω resistance. In the second case, other than having the same two-sided grounding, the armor is grounded every five kilometers. This scheme is usually used in underground cables to reduce overvoltage along the cable transmission. In the third case, the same two-sided grounding is applied to the screen and armor, while both of them are also grounded every five kilometers, to simulate the HVDC submarine cable grounding system. The distributed grounding impedance is higher than the two-sided grounding and the value of 2 Ω is considered for that. The fault is applied to the middle of the cable, which has 400 km length. Fig. 12 (a-c) depict the modal fault currents for two-sided bonding, distributed armor grounding, and distributed screen and armor grounding, respectively. Comparing the peak points of A, B, and C, there is a slight increase in the coaxial peak current, while the comparison between the points D, E, and F, shows a decrease in the peak current of the sheath mode for the distributed screen and armor grounding case. According to the figure, none of these differences makes an issue regarding the detection of modal initial peaks. It means that the impact of grounding schemes is not significant on the arrival of the modal initial peaks and proposed method can be used for different types of grounding schemes in HVDC cable bundles. It also makes sense according to Fig. 13, which shows the flowing of fault IX current into the ground for distributed grounding cases. According to the figure, the ground current amplitudes are significantly small (about 3 amps for both cases) compared to the main fault current wave reaching at the measurement point through the main conductors. This again proves that the impact of distributed grounding will not be significant on the pole values arrived at the measuring location, and consequently determined modal values. It should be mentioned that, because the connection of sheath and armor is only in discrete points, none of the modes will be eliminated. Each section has all the modes, and there will be a negligible change in the impedance at the joint locations, which does not have a significant impact on the modal behaviors and initial peak arrivals at the measurement location. However, theoretically if they are connected continually all over the cable (e.g. via a semiconducting layer) they will have the same potential and one of the modes will be eliminated.

TABLE VIII: IMPACT OF FAULT LOCATION ON THE MODAL ARRIVAL TIME IN TCE-HVDC CABLES

Fault No.	Modal time difference [μs]	Determined location [km]	Absolute relative error [%]
V	2	1.189	18.9
VI	252	149.861	0.092
VIII	470	279.503	0.17

VI. DISCUSSION

According to the results, the difference in the initial peak arrival time of the propagation modes can potentially be used for designing online fault location algorithms for HVDC cable bundles. Impact of different parameters on the modal behaviors is investigated in section IV and according to the results, the modal fault location principle is proposed for fault location in HVDC cable transmission. However, there are existing challenges in using the modal analysis of HVDC cables, which are pointed below and possible solutions are suggested for further research:

A. Proper selection of the modes:

Different pairs of modes can be used for each HVDC cable bundle to determine the transient location. The coaxial modes are always chosen as the main and the first arrival mode. The initial peak time of the second mode is compared to the coaxial mode. The second mode can be sheath/intersheath mode,

another coaxial mode, or theoretically it may even be armor/interarmor mode in case of using a robust signal-processing technique for accurate detection of the initial peaks. In some cases particularly for sheath/intersheath modes, they may arrive close to the first coaxial mode, which makes the determination of the difference in the arrival time of the modes a challenging task. In other cases mostly for armor/interarmor modes, the determination of arrival time difference is more achievable, because of the lower propagation speed in the armor/interarmor than sheath/intersheath modes. However, interarmor modal transients have small amplitudes, which makes the detection of each modal initial peak challenging. It is practically not possible to detect ground modes and they are not proper for fault localization studies. According to the aforementioned results, the selection of the second mode is a trade-off between the detection challenges due to the minor arrival time difference of the pair of modes, and small amplitude of the second mode.

B. Obtaining the modal matrix:

In the lower frequency range (less than 100 kHz), the modal speeds highly depend on the frequency used for speed calculation in (18). In fact, the characteristic ramp of velocity diagram in frequency domain may be a little different for different modes in various bundle types. It is mainly because the modes are decoupled after a certain frequency range for each cable types. In this paper, the frequency of 1 MHz is used, which guarantees the decoupling of modes for cable energization due to the high frequency of the energization transient. Looking at the modal velocities in the frequency range of more than 100 kHz in table I, the change in the velocity is not significant as frequency increases (Except cases like return mode for SCEMR cable , which the complete decoupling happens at frequency of 300 KHz. Additionally, in some other modal parameters like the ground mode attenuation, a constant increase is observed with an increase in the frequency.) This means that using the same $\boldsymbol{K_i}$ matrix with constant elements for different high- frequency transients does not lead to a significant amount of error. Accordingly, with a small acceptable error, it may be possible to directly use the resulted $\boldsymbol{K_i}$ matrices for each HVDC bundle in the decoupling process, without the need for applying the modal analysis in each sample. Additionally, the eigenvector matrices are not unique and multiple $\boldsymbol{K_v}$ and $\boldsymbol{K_i}$ matrices can be used for the modal analysis, resulting in the same decoupled modes. However, according to the proposed extensive analysis regarding the impact of different parameters like geometric, materialistic and burying configurations, they do not have a significant impact on the velocities in high frequency and the $\boldsymbol{K_i}$ matrices.

C. Significant velocity difference between the selected modes:

One of the things that should be considered is that if the velocity of the faster mode is more than three times bigger than the smaller mode, it will reach to the measurement location two times before the first arrival of the slower mode. It happens only for TCC-HVDC bundle between coaxial and intersheath modes. This reflection of the coaxial mode, may generate other modes with very small amplitude, but it will not be significant and will not have any impact on the detection for the first initial peak for the slower mode. Additionally, for the case with distributed grounding, intersheath modes with small amplitudes may be injected in the grounding points, which again does not have any impact on the detection of the modal initial peaks.

D. Impact of cable termination:

According to traveling waves theory, any change in the impedance in the transmission section, leads to into reflections and refractions. Accordingly, cable terminations will act as a change in the impedance. In this study, standard PSCAD Cable termination modeling method is used for the main conductors at the end of each cable. Additionally, the sheath and armors are grounded at the measurement location and the impact of their grounding schemes investigated in this paper. According to the results, when the first coaxial initial peak is detected, the reflection of the initial coaxial peak arrival does not have a noticeable impact on the detected initial peaks of the second and the third decoupled modal arrivals. Moreover, based on the impact of sheath/armor grounding in section V-D, and it is observed with a change in the impedance and type of grounding, the modal fault location method is feasible. Due to page limitations in-depth study of the impact of different cable terminations like outdoor terminations, GIS terminations, Dry-type plugin terminations [23] is not possible, and it is suggested to investigate in future research.

E. Feasibility of the method for multi-terminal schemes:

According to the aforementioned analysis and the explained limitations, the proposed modal fault location principle is potentially feasible for point-to-point HVDC links. As mentioned, for multi-terminal schemes, indeterminate generation of the modes in the joint locations exist due to the change in the impedance, which may make the accurate detection of modal initial peaks challenging. Even though, it does not lead to a significant accuracy decrease and still a considerable portion of the modal initial peaks travel the whole transmission grid which are clearly detectable, extensive analysis is needed for testing the feasibility of the method for multi-terminal schemes. One possible solution for dealing with this issue can be using a communication link between relays, defining multiple zones for relays, which can act as backups for the other zones leading to a selective fault location method. In this method, the time delay between modal initial peaks can be measured and compared with a predefined time setting for each relay. If the proposed method is also used for fault detection, one thing that should be cared is that the time difference between the modal initial peaks should not be significant, because after detecting the first initial peak, the fault detection algorithm must wait to detect the second reflection. According to fig. 11, this waiting time delay for a fault in 280 km from the measurement location of a TCE-HVDC cable is 470 us, which is a reasonable amount of delay for fault isolation in VSC-HVDC grids compared to the safe time limit of a few milliseconds used in literature works.

F. Impact of cable structure along the transmission section:

For the HVDC cables, which are buried underground along the whole transmission link, the modal fault localization principle can potentially give accurate results. Regarding the offshore HVDC transmission, the majority of the submarine links, have a short onshore land cable section at the end of the offshore transmission cable. Considering that in most of the cases, the onshore section is significantly short compared to the main offshore cable, the modal fault location principle can potentially

This article has been accepted for publication in a future issue of this journal, but has not been fully edited. Content may change prior to final publication. Citation information: DOI 10.1109/TPWRD.2019.2942016, IEEE Transactions on Power Delivery

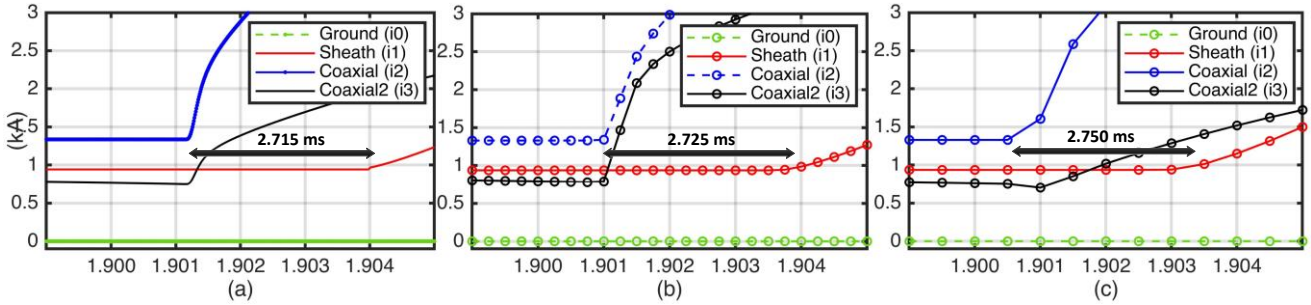

Fig. 9. Impact of sampling frequency on the modal fault location in TCC-HVDC cable. (a) 1 MHz, (b) 40 kHz, (c) 20 kHz

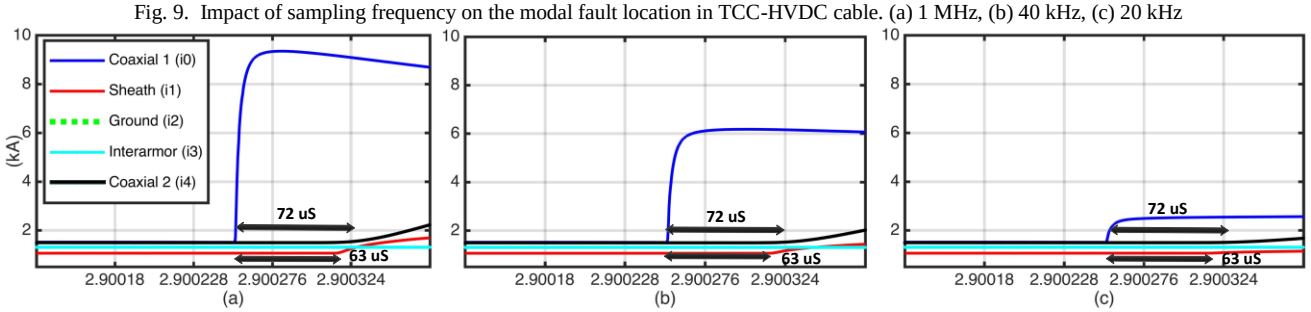

Fig. 10. Impact of fault resistance on the modal fault location in SCEMR-HVDC cable. (a) 0.1Ω (b) 1Ω (c) 100 Ω.

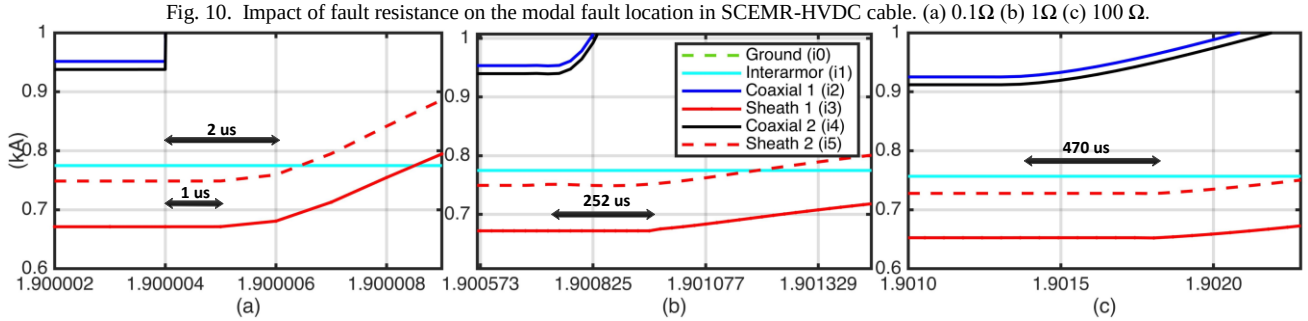

Fig. 11. Impact of fault distance on the modal fault location in TCE-HVDC cable. (a) 1 km (b) 150 km (c) 280 km

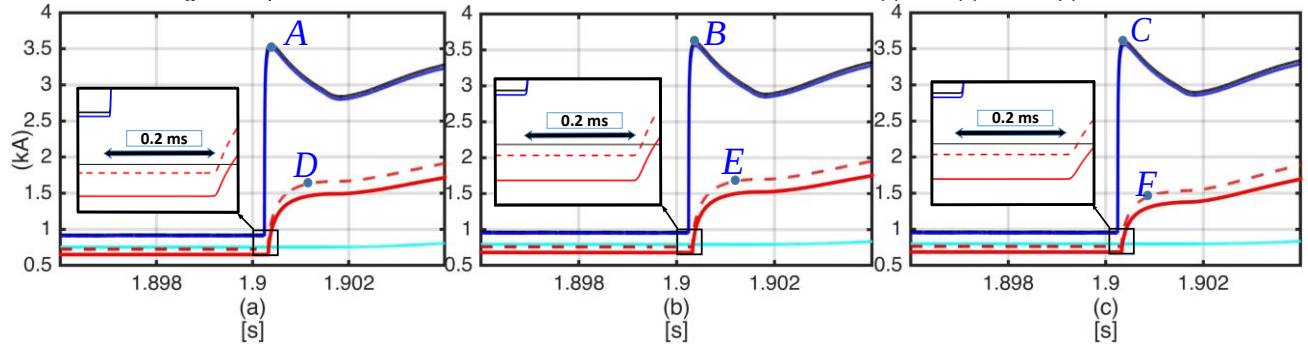

Fig. 12. Impact of the grounding scheme on the fault location in TCE-HVDC cable. (a) Two-sided bonded (b) Two-sided bonding + distributed grounding of armor (c) Two-sided bonding + distributed grounding of screen and armor

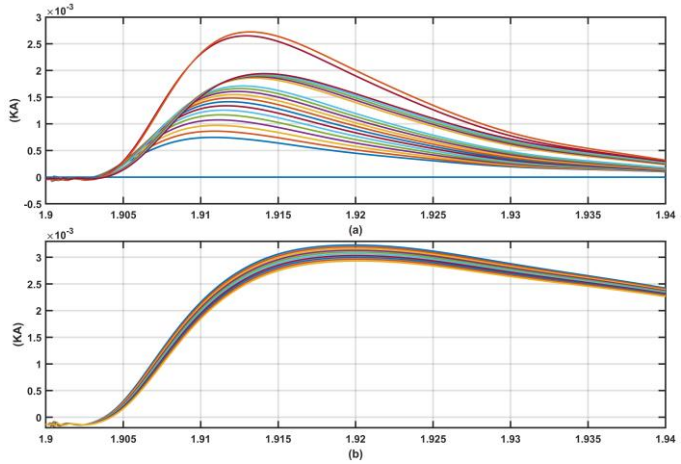

Fig. 13. Distributed ground currents in 20 ground points for TCE-HVDC cable (a) only armors grounded, (b) screen and armor connected together and then grounded.

give accurate results with negligible error. If the land cable section is long but the offshore and land cables do not have significantly different parameters, according to the sensitivity analysis given in tables II-IV regarding the layer thickness and material, the modal velocities do not significantly change with a change in these parameters. It means that still a considerable portion of the modal initial peaks arrive at the measurement location and can be accurately detected. In HVDC submarine transmission, in which different cables are used for deep and shallow water sections if the cables have significantly different parameters, the accuracy of the modal fault location may decrease. However, If the deep and shallow water sections have almost similar parameters like the Norned HVDC cable [24], the method may give satisfactory fault location results. Additionally, for HVDC cable transmission with multiple offshore and onshore sections in series like the Kontek HVDC link [25], a noticeable decrease in the accuracy of modal fault location may happen if only one set of measurement units are

used in one side of the cable. In such cases, one possible solution can be using multiple measurement sensors between the cable sections to have the most accurate modal fault location. Considering that using distributed sensors is extensively studied in literature works [7], [26], using a limited number of additional sensors can be reasonable to have the most accurate modal fault location for such mixed HVDC cable transmissions. In summary, if the modal characteristics significantly change along the transmission section, will result in noticeable decrease on the accuracy of the modal fault location. It should be noted that the aforementioned discussions are theoretical conclusions about the behavior of the modes based on the simulation results given in this paper. Further practical tests are needed to prove the accuracy of the method and design practical modal fault location schemes.

VII. Conclusion

This paper studied the modal analysis of fault transients in HVDC cable transmission. Different cable constructions with multiple layers considered as HVDC cable bundles that exist in current installations worldwide. The transformation process from the loop impedance values to series matrix and then to the decoupled modes based on the modal theory studied. Different modes with the corresponding equivalent circuits presented for each cable bundle. The frequency characteristic of modal attenuation and speeds for different HVDC cable bundles studied and the impact of different parameters on the modal behavior analyzed. A concept for fault localization in HVDC cables based on the difference in arrival times of fault transients due to the difference in the modal velocities introduced. The proposed method uses one-sided measurement without needing a communication link or any detection for the second TW reflections. Multiple faults applied to CIGRE HVDC models and the impact of different parameters analyzed. It has been resulted that different cable parameters, dimensions, and burial configurations, do not have a significant impact on the resulted modal matrices and consequently further modal fault localization algorithm. The proposed technique accurately works for high impedance faults and for long distance faults. The modal fault location principle can be obtained using lower sampling frequencies with an acceptable error value. Different grounding schemes may have a slight impact on the detection of the modal initial peaks and inject small intersheath modal transients, but this impact is not significant on the feasibility of the fault localization algorithm. The proposed study can be used as reference work for designing protection algorithms for HVDC transmission systems using AI-based techniques or signal processing methods. Accordingly, further works consist of implementing the online fault localization algorithm based on the proposed modal principle, using robust signal processing techniques for designing the fault location algorithms, and studying the impact of errors due to sensor measurement. Impact of distortion in the accuracy of the further designed modal online fault locators should be analyzed. The challenges pointed in the discussion section must be analysed for the final designed modal protection schemes. The proposed analysis may also be extended to multi-terminal VSC-HVDC grids for both selective fault detection and fault localization, which have more complicated fault scenarios and the modal behaviors will be more complex. Accordingly, testing and analyzing the modal online fault localization algorithm with several fault events having different impedances, types, and locations may also prove the accuracy of the method for multi-terminal HVDC connections.

References

[1] C. F. Jensen, *Online Location of Faults on AC Cables in Underground Transmission Systems*. 2014.

[2] G. Y. Kwon *et al.*, "Offline fault localization technique on HVDC submarine cable via time-frequency domain reflectometry," *IEEE Trans. Power Deliv.*, vol. 32, no. 3, pp. 1626–1635, 2017.

[3] M. Bawart, M. Marzinotto, and G. Mazzanti, "Diagnosis and Location of Faults in Submarine Power Cables," pp. 24–37, 2016.

[4] G. Kwon, C. Lee, G. S. Lee, Y. H. Lee, S. J. Chang, and C. Jung, "Offline Fault Localization Technique on HVDC Submarine Cable via Time – Frequency Domain Reflectometry," vol. 32, no. 3, pp. 1626–1635, 2017.

[5] Y. Hao, Q. Wang, Y. Li, and W. Song, "An intelligent algorithm for fault location on VSC-HVDC system," *Int. J. Electr. Power Energy Syst.*, vol. 94, pp. 116–123, 2018.

[6] J. Li, Q. Yang, H. Mu, S. Le Blond, and H. He, "A new fault detection and fault location method for multi-terminal high voltage direct current of offshore wind farm," *Appl. Energy*, vol. 220, pp. 13–20, Jun. 2018.

[7] W. Leterme and D. Van Hertem, "Cable Protection in HVDC Grids Employing Distributed Sensors and Proactive HVDC Breakers," *IEEE Trans. Power Deliv.*, vol. 33, no. 4, pp. 1981–1990, Aug. 2018.

[8] N. M. Haleem and A. D. Rajapakse, "Local measurement based ultra-fast directional ROCOV scheme for protecting Bi-pole HVDC grids with a metallic return conductor," *Int. J. Electr. Power Energy Syst.*, vol. 98, no. December 2017, pp. 323–330, 2018.

[9] A. Hossam-Eldin, A. Lotfy, M. Elgamal, and M. Ebeed, "Artificial intelligence-based short-circuit fault identifier for MT-HVDC systems," *IET Gener. Transm. Distrib.*, vol. 12, no. 10, pp. 2436–2443, May 2018.

[10] Y. Li, Y. Gong, and B. Jiang, "A novel traveling-wave-based directional protection scheme for MTDC grid with inductive DC terminal," *Electr. Power Syst. Res.*, vol. 157, pp. 83–92, 2018.

[11] S. H. Ashrafi Niaki, S. A. Nabavi Niaki, and A. A. Abdoos, "Fault detection of HVDC cable in multi-terminal offshore wind farms using transient sheath voltage," *IET Renew. Power Gener.*, vol. 11, no. 13, pp. 1707–1713, 2017.

[12] A. Ametani, T. Ohno, and N. Nagaoka, *Cable System Transients: Theory, Modeling and Simulation*. Singapore: John Wiley & Sons, Singapore Pte. Ltd, 2015.

[13] A. Wasserrab and G. Balzer, "The significance of frequency-dependent overhead lines for the calculation of HVDC line short-circuit currents," *Electr. Eng.*, vol. 97, no. 3, pp. 213–223, Sep. 2015.

[14] N. Tong *et al.*, "Local Measurement-Based Ultra-high-speed Main Protection for Long Distance VSC-MTDC," *IEEE Trans. Power Deliv.*, vol. PP, no. c, pp. 1–1, 2018.

[15] R. Benato, M. Forzan, M. Marelli, A. Orini, and E. Zaccone, "Harmonic behaviour of HVDC cables," *Electr. Power Syst. Res.*, vol. 89, pp. 215–222, 2012.

[16] E. Stern *et al.*, "B4-118 CIGRE 2008 THE NEPTUNE REGIONAL TRANSMISSION SYSTEM 500 kV HVDC PROJECT," pp. 1–8, 2008.

[17] C. Harvey, "The Moyle HVDC Interconnector: Project Considerations, Design and Implementation," *IEE Conf. AC-DC Power Transm.*, vol. 485, no. 485, pp. 145–148, 2001.

[18] F. F. da Silva and C. L. Bak, *Electromagnetic Transients in Power Cables*, vol. 72. 2013.

[19] Lauha Fried, "Stability and control of mixed AC-DC systems with VSC-HVDC: a review," *Glob. Wind Energy Counc.*, vol. 12, p. 76, 2017.

[20] A. Wasserrab and G. Balzer, "Frequency-dependent cables for the calculation of line short-circuit currents in HVDC networks," *Proc. Univ. Power Eng. Conf.*, no. 1, pp. 0–5, 2014.

[21] T. K. Vrana, *The Cigré B4 DC grid test system The CIGRE B4 DC Grid Test System B4-57*, no. August. 2015.

[22] C. V. T. M. Szechtman, T. Wess, "First Benchmark Model for HVDC Control Studies," *CIGRE Electra*, vol. 135, 1991.

[23] H. Ye *et al.*, "Review on HVDC cable terminations," *High Volt.*, vol. 3, no. 2, pp. 79–89, 2018.

[24] J.-E. Skog, K. Koreman, B. Pääjärvi, T. Worzyk, and T. Andersröd, "The Norned HVDC cable link--A power transmission highway between Norway and The Netherlands," *Energex 2006*, no. January 2006, pp. 239–278, 2006.

[25] C. Wolff and T. Elberling, "The Kontek HVDC link between Denmark and Germany," in *2000 IEEE Power Engineering Society Winter Meeting. Conference Proceedings (Cat. No.00CH37077)*, vol. 1, pp. 572–574.

[26] D. Tzelepis *et al.*, "Single-ended differential protection in MTDC networks using optical sensors," *IEEE Trans. Power Deliv.*, vol. 32, no. 3, pp. 1605–1615, 2017.

Mani Ashouri received his B.Sc. and M.Sc. from Babol University of technology, Iran. He is currently a Ph.D. student in the Department of Energy Technology, Aalborg University, Denmark. He had been working as HVAC protection and relay test engineer during 2011-2017 in Iranian northern TSO. His main research interests are protection and control of multi-terminal VSC-HVDC and HVAC systems, Electromagnetic transients in electrical power systems and high voltage cables, power electronic converters used for HVDC transmission and signal processing methods for power system fault analysis.

Filipe Faria da Silva received his M.Sc. in Electrical and Computers Engineering in 2008 from Instituto Superior Tecnico, Portugal, and his Ph.D. in Electric Power Systems in 2011 from Aalborg University, Denmark. He was with EDP-Labelec in 2008 and with the Danish TSO Energinet from 2008 to 2011. He is currently Associate Professor at the Department of Energy Technology, Aalborg University, where he is also semester coordination for the Electrical Power System and High Voltage Engineering master program and vice-leader of the Modern Power Transmission Systems research program. His research focuses on power cables, electromagnetic transients, system modeling, network stability, HVDC transmission, and HV phenomena. Filipe is an active member of CIGRE and IEEE, being currently head of Denmark's IEEE-PES, the Danish representative for CIGRE SC C4 System Technical Performance and the convener of CIGRE WG C4.46.

Claus Leth Bak was born in Arhus, Denmark in 1965. He is currently a Professor in the Department of Energy Technology at Aalborg University, Denmark. His main research areas include corona phenomena on overhead lines, power system modeling and transient simulations, underground cable transmission, power system harmonics, power system protection, and HVDC-VSC offshore transmission networks. He is a member of CIGRE JWG C4-B4.38, CIGRE SC C4, and SC B5 study committees member and chairman of Danish CIGRE National Committee. He serves as Head of the Energy Technology Ph.D. program and as Head of the Section of Electric Power Systems and High Voltage in Aalborg University and is a member of the Ph.D. board at the Faculty of Engineering and Science.